IEEE Access
Multidisciplinary | Rapid Review | Open Access Journal

Received December 28, 2019, accepted January 18, 2020, date of publication January 31, 2020, date of current version February 10, 2020.

Digital Object Identifier 10.1109/ACCESS.2020.2970769

On the Impact of the Radiation Pattern of the Antenna Element on MU-MIMO Indoor Channels

JESÚS R. PÉREZ AND RAFAEL P. TORRES
Department of Communications Engineering, Universidad de Cantabria, 39005 Santander, Spain
Corresponding author: Jesús R. Pérez (jesusramon.perez@unican.es)

This work was supported by the Spanish Ministerio de Economía, Industria y Competitividad, under the project TEC2017-86779-C2-1-R.

ABSTRACT This paper presents an analysis of the effect that the radiation pattern of the antenna element that makes up the base station array has on the structure of multi-user multiple-input multiple-output (MU-MIMO) channels. In this paper, the analysis focuses on the uplink. It is well known that the antennas are an inseparable part of the radio channel. The use of more or less directional antennas as elements of the base station array of a MIMO system influences the channel in two fundamental parameters that affect the performance of MU-MIMO systems: on the one hand, the coherence bandwidth, which determines the necessary overhead in the channel estimation; and, on the other hand, the orthogonality of the subchannels between the multiple users and the base station, which influences the degree with which the condition of ''favorable propagation'' is fulfilled. Based on an experimental analysis using both omnidirectional and directional antennas, conclusions are drawn about how these two parameters are affected and their influence on the spectral efficiency obtainable. The measurement campaign was carried out in an indoor environment in the 3 to 4 GHz band.

INDEX TERMS 5G mobile systems, channel capacity, frequency selectivity, massive MIMO, multi-user MIMO.

I. INTRODUCTION

The development of the fifth generation of mobile communications systems (5G) requires not only the availability of more spectrum to meet both the 5G usage scenarios and to enable the key capabilities of IMT-2020 [1], but also the optimum use of the radio channel, enhancing the spectral efficiencies. Among others, one of the key technologies considered for increasing spectral efficiency will be the evolutions of the multiple input and multiple output (MIMO) systems, originally designed for point-to-point communications [2], [3]. Subsequently, the concepts of multi-user MIMO were developed [4]–[6], which currently have massive MIMO systems as one of their most promising form [7]–[13].

The achievable capacity in a specific MU-MIMO channel depends on the extent to which the ''favorable propagation'' condition is met. This consists in that the channels established between different user terminals (UTs) and the base station (BS) are orthogonal to each other. Moreover, it is assumed that this orthogonality increases as the number of antennas considered at the BS also grows.

The associate editor coordinating the review of this manuscript and approving it for publication was Hassan Tariq Chattha.

Antennas are an inseparable part of the radio channel; their radiation pattern and polarization highly influence the response of the channel and thus, the degree of achievement of the condition of favorable propagation. Therefore, the selection of the type of antenna is an aspect of great interest both in the field of MU-MIMO [10], [11], and for the development of MIMO systems based on spatial modulation (SM-MIMO) [14], [15]. In MIMO systems, the influence of the antenna element on their performance has been widely studied, mainly from the point of view of the impact of antenna coupling in the system, as in [16]–[20].

If we focus on the up-link, the radiation pattern of the antenna element of the BS behaves as a spatial filter that attenuates the signals coming from some directions of arrival (DoA) and amplifies others. If we consider a propagation environment rich in scattering, and in which all the DoA are equiprobable, it can be stated that the use of directional antennas will reduce the richness of scattering at the receiver against the use of less directional or omnidirectional ones. In a real indoor environment, the above statement will generally be true, although there may be some exceptions; for example, when the most relevant contributions of the multi-path have their DoA lying in the main lobe of the directional antenna.

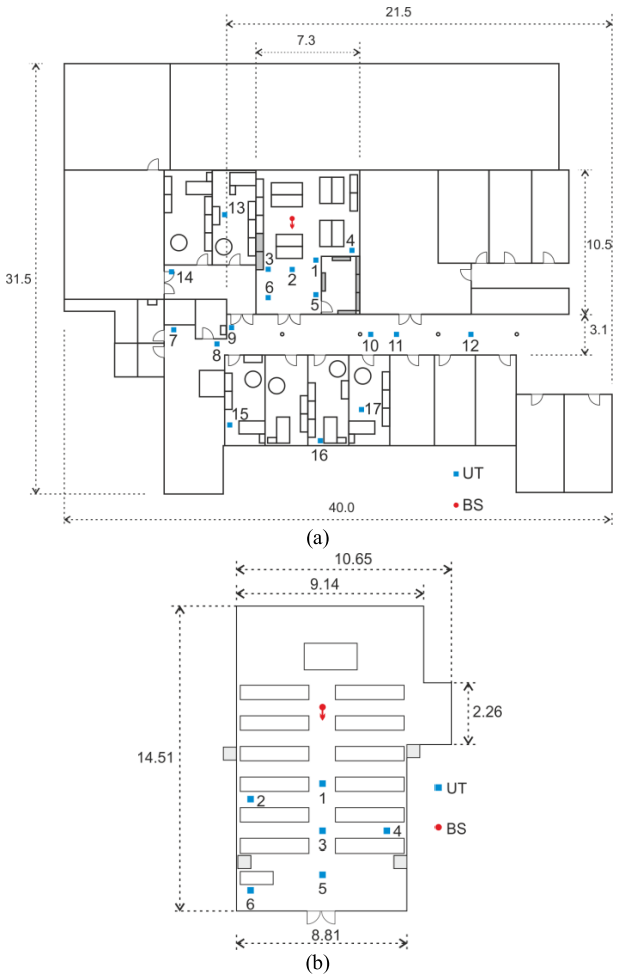

FIGURE 1. Indoor environments, dimensions in meters. The arrow shows the Rx broadside direction. (a) Site 1 top view, detail of UT_{1-17} positions. (b) Site 2 top view, detail of UT_{1-6} positions.

The reduction of multipath components has, a priori, two consequences on the radio channel: on the one hand, the positive side is that the frequency selectivity of the channel is reduced because its impulse response will have fewer components; on the other hand, the lower richness of scattering can lead, with high probability, to a reduction of the orthogonality of MU-MIMO channels.

In addition, the use of directive antennas could have a third effect on the MU-MIMO channel matrix, which is to accentuate the power imbalance between the different sub channels. From the point of view of the up-link, the difference in powers received by the BS from each one of the active users would be increased by using directive antennas. In a real environment, the degree to which these three effects occur is difficult to assess a priori.

In this paper, we present the results of measurement campaigns that allow us to confirm experimentally these effects, and the degree to which they are verified in a propagation environment and for a specific frequency band. Obviously, the aim is to make a meaningful contribution, although more experimental data would be required to perform a complete analysis of the impact that the radiation pattern of the antenna array element has on the MU-MIMO and SM-MIMO systems.

The results presented in this paper correspond with new measurement campaigns carried out in two propagation environments that complement those already carried out in the same scenarios in the 3 to 4 GHz band [21], [22], now using a directional ultra-wideband antenna as the main element of the BS antenna array, instead of the omnidirectional one, and including some new UT locations in the study. In [21], an analysis of indoor broadband channel parameters such as the wideband propagation losses, the variations in the mean square delay spread along with the coherence bandwidths between the receiver omnidirectional array antenna elements, or the correlation between the channels established between each UT and the multiple antennas that make up the virtual array is presented. However, the analysis of the capacity of the MU-MIMO channel requires it to be taken into account that there will be several UTs simultaneously active, and analyzing the orthogonality of the MU-MIMO channel matrix and thus, the degree of compliance with the condition of ''favorable propagation'', as presented in [22].

This paper investigates the influence on the MU-MIMO channel of the directivity of the type of antenna element considered for the BS array, using to quantify these differences the following fundamental parameters: the coherence bandwidth, the condition number of the channel matrix and the achievable up-link sum capacity of the system when using both omnidirectional and directional antennas. Section II describes the measurement environments and set-up configuration. Section III presents the MU-MIMO channel model considered. Section IV includes a discussion of the results achieved, underlining the differences between both types of antennas considered and, finally, the most representative conclusions are outlined in Section V.

II. INDOOR CHANNEL MEASUREMENTS

The indoor measurement campaigns have been carried out at the Ingeniería de Telecomunicación ''Profesor José Luis García García'' building at the University of Cantabria, considering the scenarios shown in Fig. 1, [21]. The building has concrete floors, ceiling boards, drywalls and metallic doors for all of the indoor rooms.

Site 1 shown in Fig. 1(a) includes offices with wooden furniture, a central corridor and the computer laboratory in which the receiver antenna (Rx) is located, with the presence of metallic bookshelves (those shadowed in gray). The second environment, Site 2 shown in Fig. 1(b), is a meeting room with almost uniformly spaced rows of desks and chairs.

Fig. 1 includes a summary of the transmitter antenna (Tx) positions, i.e. UT positions, considered in the analysis for both scenarios, making it possible to differentiate in Fig. 1(a) for Site 1 two sets of UT locations: 1) UT_{1-6} positions under line-of-sight (LOS) conditions and, 2) UT_{7-17} positions under non-LOS (NLOS) conditions and with a different

degree of obstruction. Concerning Site 2, 6 UT positions (UT_{1-6}) under LOS conditions have been considered. Concerning the UT-BS distances for both environments, they lie in the range [3.6-6.1 m] and [5.0-16.1 m] for Site 1 on LOS and NLOS conditions, respectively; and [3.7-9.1 m] for Site 2 LOS cases.

For both measurement scenarios, it should be noted that the average signal to noise ratio (SNR) over all the BS antenna elements is 35 dB. For the capacity analysis, a SNR value of 10 dB has been chosen.

The measurement system utilized to carry out the channel measurements consists of a planar scanner with two servomotors, along with a vector network analyzer (VNA), both remote controlled. The planar scanner makes up the virtual array (VA) at the receiver side [21].

At each receiver antenna position (Rx) of the measurement vertical plane, the S_{21}-trace is acquired from the VNA and its post-processing makes it possible to obtain the channel transfer function of the wideband channel and from it, a complete characterization of the channel established between any UT/Tx and the Rx/BS VA.

The measurements have been carried out in the 3 to 4 GHz frequency band, with $N = 801$ frequency tones for the S_{21}-trace, and considering a height of 1.5 m for both antennas, UT and the BS center position of the VA. For any of the UT positions, the VA scanning area is 126×126 mm in size (7×7 points $\lambda/4$ spaced at 3.5 GHz).

In this work, the effect of the receiver antenna has been investigated, using in the measurement campaigns two different types of ultra-wideband antennas at the BS side: 1) an EM-6865 omnidirectional biconical antenna (2-18 GHz) with an average 2.1 dBi gain in the frequency range considered and, 2) a HG2458-08LP 8 dBi directional log periodic antenna (2.4-5.8 GHz) with a front to back ratio higher than 20 dB and horizontal and vertical beam widths of 80 and 60 degrees, respectively. The omnidirectional antenna has a radiation pattern similar to a $\lambda/2$ dipole, i.e., an isotropic horizontal plane and a vertical beam width of approximately 80 degrees. The log periodic antenna has a medium directivity, but practically all the power is radiated forward. Regarding the transmitter antenna (Tx), which emulates the antenna of any UT, a second omnidirectional EM-6865 antenna has been used.

Finally, it must be pointed out that the measurements have been carried out at night to guarantee stationary conditions, as the influence of people on channel performance is beyond the scope of this research.

III. MU-MIMO CHANNEL MODEL

The multi-user channel matrix mathematically represents the set of radio channels that are established between the antenna of a number of active UTs and each one of the BS antenna array elements. Fig. 2 shows a scheme of a MU-MIMO configuration, in which the elements of the vectors $\boldsymbol{H}_q$ are the scalar channels established between the q-th active UT and the m-th element of the BS antenna array (H_q^m),

$$\boldsymbol{H}_q = \left(H_q^1,\ H_q^2, \ldots, H_q^m, \ldots, H_q^M\right); \quad q = 1, \ldots, Q \tag{1}$$

where M represents the number of antennas of the receiver array, i.e. $M = 49$ in this work. This is valid for any of the k measured frequency tones.

We define the channel matrix $\aleph[k]$, as commonly accepted, so that each one of its columns represents the narrowband channel $\boldsymbol{H}_q[k]$ of order $M \times 1$ corresponding to the k-th frequency tone of the q-th active UT. As a result, the channel matrix is of order $M \times Q$, Q being the number of simultaneously active UTs.

When the measurement set-up is properly calibrated at the transmitter and receiver radiofrequency cable ends, the elements of the matrix $\aleph[k]$ are directly obtained from the VNA measured S-trace as given by:

$$H_q^m[k] = S_{21}^{qm}[k], \tag{2}$$

in which $S_{21}^{qm}[k]$ is the scattering parameter of the k-th tone measured with the VNA when the q-th UT is transmitting and the m-th antenna element of the BS array is considered at the receiver side. Thus, H_q^m is the channel transfer function (CTF) of the scalar channel established between the pair of antennas (q,m).

From the knowledge of the CTF, we can obtain the channel impulse response of each scalar channel by applying the inverse Fourier transform to the measured CTF, that is,

$$h_q^m[n] = \frac{1}{N} \sum_{k=0}^{N-1} W[k]\ H_q^m[k] \exp\left(j\frac{2\pi}{N}kn\right). \tag{3}$$

In (3), $W[k]$ represents a Hamming window applied to the measured CTF in order to reduce sidelobe levels in the time-domain impulse response. Finally, the Power Delay Profile (PDP) is obtained from the impulse response as:

$$P[n] = |h[n]|^2. \tag{4}$$

Once the PDP is known for each one of the $M \times Q$ scalar channels, we can obtain the main wideband channel parameters, the RMS delay spread and the coherence bandwidths (B_C), and analyze their behavior in both the local area of the array and the entire measurement environment. A detailed analysis of these parameters and their relationships has already been carried out by the authors for omnidirectional antennas [21]. In this work, with the aim of investigating the effect of the radiation pattern of the BS basic antenna array element, we will focus on analyzing the coherence bandwidths for both channels: those associated with the use of an omnidirectional antenna, called hereinafter omnidirectional channels (OCh); and the so-called directive channels (DCh), corresponding with the use at the BS of a directional antenna. In the case of wide-sense stationary uncorrelated scattering (WSSUS) channels, the autocorrelation function of the channel is obtained by means of the Fourier Transform of the PDP. Once obtained and normalized to its maximum value at the origin, the values of B_C at different correlation levels

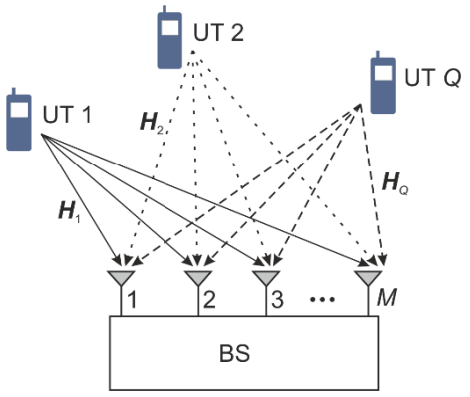

FIGURE 2. MU-MIMO scheme particularized for the up-link.

are obtained as the bandwidth over which the correlation function is above a predetermined level, 0.7 in our case [23].

With the intention of comparing both OCh and DCh channels, we will focus on calculating the condition number along with the sum capacity for the up-link channel. The channel sounding measurement set-up considered emulates a simple cell system with the BS equipped with a rectangular array of $M = 49$ antennas, the number of active users is $Q = 6$, and each UT is equipped with only one antenna. We consider that the BS knows the channel and that the UTs are not collaborating among each other. Moreover, we consider an OFDM system with N subcarriers, which corresponds with the 801-frequency measured tones.

The signal received at the BS for the k-th subcarrier when the Q users are simultaneously transmitting is given by

$$\boldsymbol{y}[k] = \sqrt{SNR}\,\boldsymbol{G}[k]\;\boldsymbol{s}[k] + \boldsymbol{n}[k]; \quad k = 1, ..., N \tag{5}$$

where $\boldsymbol{y}[k]$ is a column vector with M elements corresponding to the k-th subcarrier, $\boldsymbol{G}[k]$ is the normalized channel matrix, of order $M \times Q$, in which each one of its columns represents the narrowband channel ($\boldsymbol{g}_q[k]$) of order $M \times 1$ corresponding to the k-th subcarrier. The signals transmitted from each UT are grouped into the signal vector $\boldsymbol{s}$ ($Q \times 1$) that is normalised so that $\mathrm{E}\{||\mathbf{s}||^2\} = 1$; and, finally, $\boldsymbol{n}$ ($M \times 1$) is a complex Gaussian noise vector with i.i.d. unit variance elements. The SNR represents the mean signal to noise ratio at the receiver.

The matrix $\boldsymbol{G}[k]$ in (5) is normalised in such a way that it verifies:

$$\mathrm{E}\left\{ \|\boldsymbol{G}\|_{\mathrm{F}}^{2} \right\} = M \cdot Q \tag{6}$$

where $\|\|_{\mathrm{F}}$ represents the Frobenious norm of a matrix, and $\mathrm{E}\{\ .\ \}$ is the expected value operating over the frequency.

In our case, the matrix $\boldsymbol{G}[k]$ is obtained from the matrix of the raw channel measurements ($\aleph[k]$) by means of a normalization process:

$$\boldsymbol{G}_{M\times Q} = \aleph_{M\times Q}\,\boldsymbol{J}_{Q\times Q} \tag{7}$$

The normalization matrix $\boldsymbol{J}$ is a diagonal matrix of order $Q \times Q$, whose elements (j_q) can be chosen in two different ways that we will denote as normalization 1 (N1) and normalization 2 (N2), following the nomenclature proposed in [10], and given according to (7) and (8), respectively. Both N1 an N2 normalizations verify (6).

$$j_q = \sqrt{\frac{M}{\frac{1}{N}\sum_{k=1}^{N} \left|\boldsymbol{H}_q[k]\right|^2}}; \quad q = 1, \ldots, Q \tag{8}$$

$$j_q = \sqrt{\frac{M\,Q}{\frac{1}{N}\sum_{k=1}^{N} \left\|\aleph_q[k]\right\|_{\mathrm{F}}^2}}; \quad q = 1, \ldots, Q \tag{9}$$

When N2 is used, all the elements of the diagonal matrix $\boldsymbol{J}$ (9) are equal, and thus the operation in (7) is equivalent to multiply the matrix by a scalar. This normalization preserves the original structure of the measured channel matrix, i.e. it keeps the difference between the received power from different UTs, receiver antennas and frequency tones.

However, if we use N1 as given in (8), the elements of the diagonal matrix $\boldsymbol{J}$ take different values; in this case, the power imbalance between the channels corresponding to each UT is eliminated, although the channel variations between antennas within the receiver array and frequency tones are maintained.

N1 changes the original structure of the radio channel. We can interpret that the resulting normalized matrix, $\boldsymbol{G}$, corresponds with a system in which an ideal power control is performed. In this case, the total available power transmitted by the users is not distributed equally, but each UT is assigned the necessary power so that all UTs reach the BS with the same power.

The spectral efficiency that MU-MIMO systems can theoretically achieve depends largely on the degree to which the condition of "favorable propagation" is met, which depends on the extent to which the channels of the different users are orthogonal [7]–[11]. A commonly accepted metric used to weigh up the orthogonality of the columns of a matrix is the condition number, κ, which is also a measure of the dispersion of the singular values of the matrix. The condition number of a matrix $\boldsymbol{G}$ is defined by the relationship:

$$\kappa = \frac{max\left\{eigenvalue\left(\boldsymbol{G}^H\,\boldsymbol{G}\right)\right\}}{min\left\{eigenvalue\left(\boldsymbol{G}^H\,\boldsymbol{G}\right)\right\}}. \tag{10}$$

It is important to take into account the effect that the normalization of $\boldsymbol{G}$ introduces in κ. If we use N1, the norm of all columns in $\boldsymbol{G}$ are equal, and κ is a valid measure of the orthogonality of the columns of $\boldsymbol{G}$. According to (10), a value of κ equal to one corresponds to a channel matrix in which all its columns are orthogonal. Conversely, high values of κ indicate that at least two columns of the matrix will be practically collinear. It is more suitable in order to interpret the results to use the inverse of the condition number (ICN), which varies between 1 (maximum orthogonality) and 0 (zero orthogonality). On the contrary, if we use N2, the imbalance between the norms of the columns in $\boldsymbol{G}$ is maintained. In this case, κ is a valid measure of

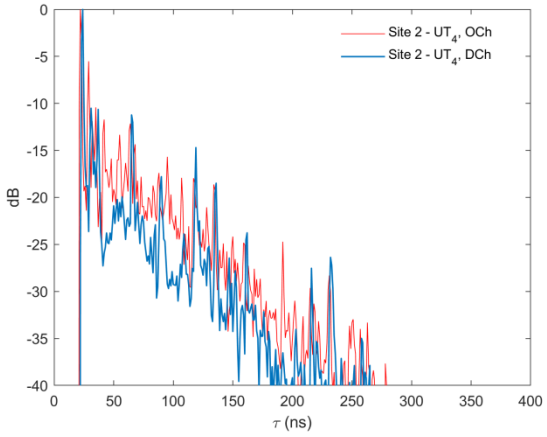

FIGURE 3. PDP obtained at Site 2 for the UT_4 position.

the dispersion of the eigenvalues of $\boldsymbol{G}^{\mathrm{H}}\boldsymbol{G}$, but no longer of the orthogonality, since the dispersion of the eigenvalues can be due to both the power imbalance as well as the lack of orthogonality.

The statistical distribution of the condition number or its inverse, using N1, are valid metrics of the degree to which the condition of "favorable propagation" is met, but they are not a direct measure of the goodness of the channel in terms of the spectral efficiency achievable in bits/s/Hz. Therefore, to have a complete view of the difference between both OCh and DCh, and the impact of the antennas in the MU-MIMO system, we calculate the sum capacity for both channels, specifically for the up-link case.

To calculate the capacity we assume a MU-MIMO system operating on an OFDM basis as defined previously (5). Under these assumptions, we obtain the sum capacity of the MU-MIMO system by means of the decomposition in singular values of the channel matrix:

$$C\ [k]=\sum_{q=1}^{Q} log_2\left(1+\frac{SNR}{Q}\lambda_q\right);\quad k=1,2,\ldots,N \qquad (11)$$

in which λ_q represents the q-th eigenvalue of the $\boldsymbol{G}^{\mathrm{H}}\boldsymbol{G}$ matrix, i.e. the square of the q-th singular value of the $\boldsymbol{G}$ matrix.

IV. RESULTS

In this section, the OCh and DCh channels are compared based on the statistical distribution of the most relevant channel parameters, i.e., B_C, ICN, and sum capacity (C). The inverse condition number as well as the sum capacity have been obtained by applying both normalizations N1 and N2. In addition, the comparison is made for the two measurement environments considered, differentiating both LOS and NLOS situations. The coherence bandwidth has been considered for a correlation value of 0.7, an intermediate value between 0.5 and 0.9. The number of active UTs is set to $Q = 6$ for all cases.

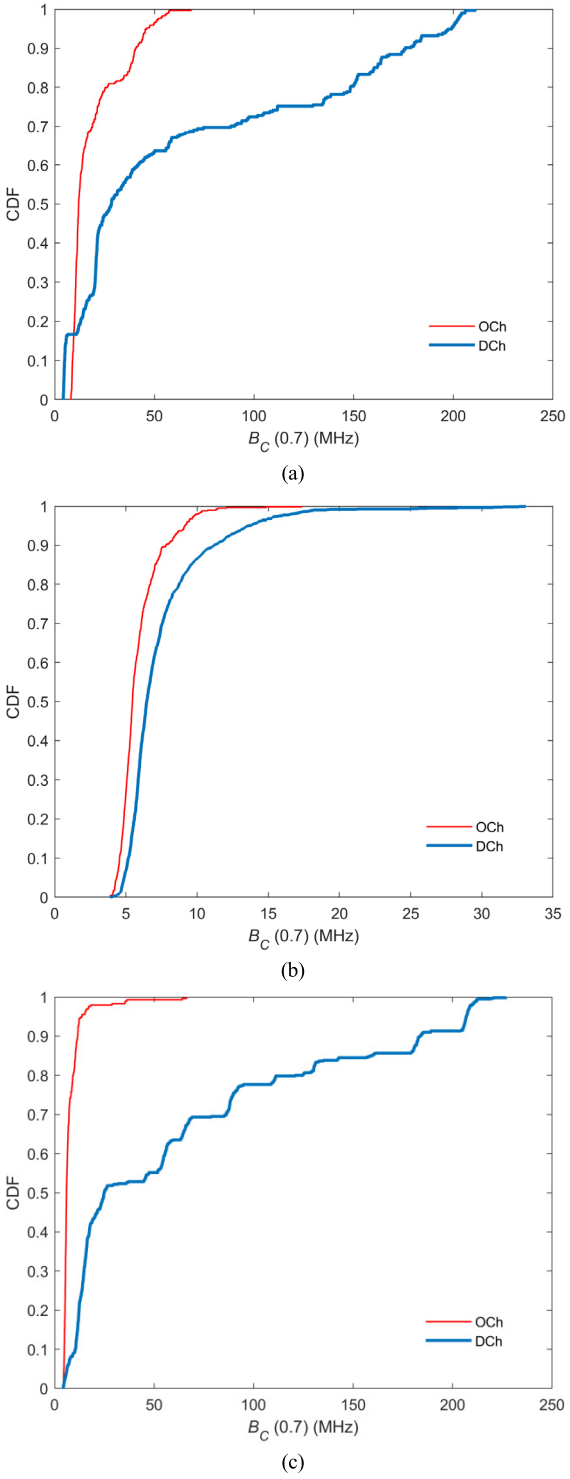

FIGURE 4. CDF of the B_C for a correlation factor of 0.7. (a) Site 1–LOS (UT_{1-6}). (b) Site 1–NLOS (UT_{7-17}). (c) Site 2–LOS (UT_{1-6}).

A. COHERENCE BANDWIDTH

The B_C of a channel is a measure of its frequency selectivity, and maintains an inverse relationship with the temporal dispersion. In Fig. 3, we present a comparison between the PDP obtained for OCh and DCh and a UT under LOS conditions.

The result shown is representative of what happens as a general trend for the rest of the measured UTs positions. The DCh can be considered a filtered version of the OCh, and it is observed how some multipath components are attenuated, and, in a smaller number, others are amplified depending on their DoA. At first glance, it can be stated that the OCh is more dispersive than the DCh.

A rigorous analysis requires the comparison of more cases through a quantifiable parameter, such as the B_C. In Fig. 4, the cumulative distribution function (CDF) of the coherence bandwidth for a correlation level of 0.7 and for both channels, OCh and DCh, is presented for all the situations. The CDFs are obtained on the set of 294 subchannels measured in each situation, $Q \times M$, being $Q = 6$ and $M = 49$ in our case.

For the three situations, it is observed as a general trend that the use of a directional antenna at the BS gives rise to a channel (DCh) with greater coherence bandwidth values than when using an omnidirectional antenna (OCh). For the LOS case, in Site 1 and according to Fig.4(a), there is a 16.6% probability that the OCh has B_C values slightly higher than the DCh. However, for most situations the DCh channel has far higher B_C values. For the NLOS situation, in Fig.4(b), the DCh always exhibits a lower frequency selectivity, although the difference between the B_C values in both channels is lower than in the LOS case. Finally, in Fig.4(c) the result obtained in Site 2 under LOS conditions is presented. The results are similar to that obtained in the LOS case in Site 1, although in this case the B_C of the directional channel is always greater than that achieved with the omnidirectional one.

B. INVERSE CONDITION NUMBER

Fig. 5 shows the CDFs of the ICN of the MU-MIMO channel with six active UTs for the three situations considered. The results also include a theoretical reference channel where all the elements of the $\boldsymbol{G}$ matrix are independent, identical distributed, zero-mean complex Gaussian, unit-variance random variables (i.i.d. Rayleigh).

The results for the Site 1-LOS environment are presented in Fig. 5(a). It can be observed that when we normalize the measured channel matrix ($\aleph$) according to the N2 normalization, i.e. maintaining the structure of the measured channel, the OCh channel has higher ICN values than the DCh one. On the contrary, if we use the N1 normalization, equivalent to performing an ideal power control, the situation is reversed and the DCh channel has higher ICN values than the OCh one. In both OCh and DCh, the normalization N1 leads to lower dispersion of the singular values than for the N2 case. However, the effect is greater for the DCh channel.

Fig. 5(b) shows the results for the Site 1-NLOS environment. As in LOS, the N1 normalization shows a lower dispersion of the singular values than the N2. However, unlike LOS, the OCh channel has higher ICN values, i.e. a smaller dispersion of the singular values than the DCh one.

Finally, Fig. 5(c) shows the results achieved for another LOS situation, but in Site 2. Although the results follow the trend of the previous case (Site 1-NLOS), it can be observed that the differences between N1 and N2 are less than in the previous cases. This fact indicates that the power imbalance between users is also lower in this environment.

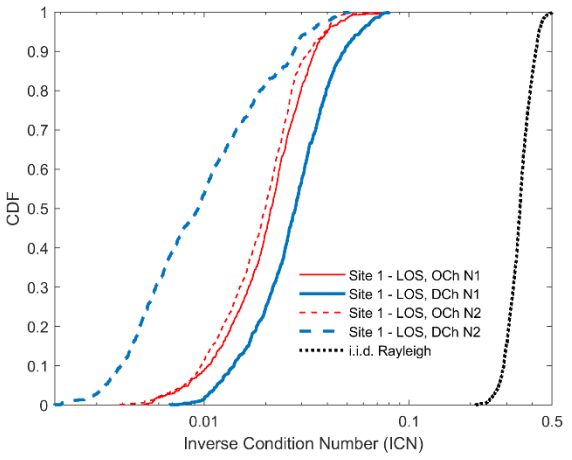

FIGURE 5. CDF of the ICN for 6 active UTs and 49 elements at the BS. (a) Site 1–LOS (UT_{1-6}). (b) Site 1–NLOS (UT_{7-17}). (c) Site 2–LOS (UT_{1-6}).

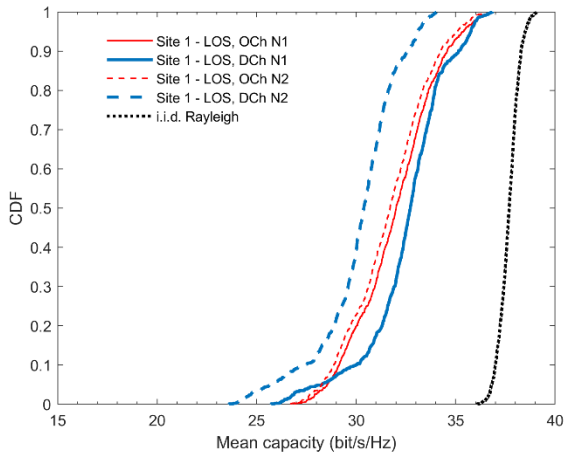

(a)

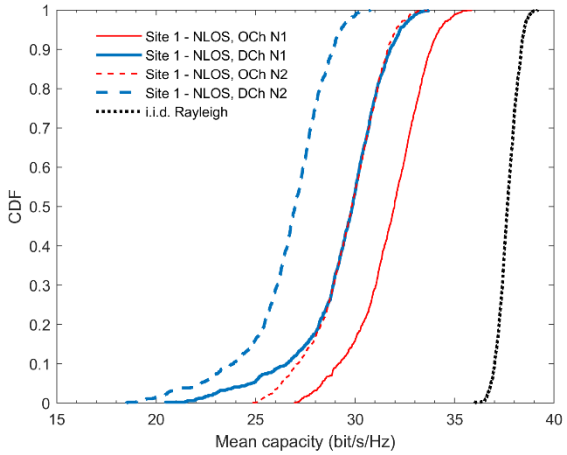

(b)

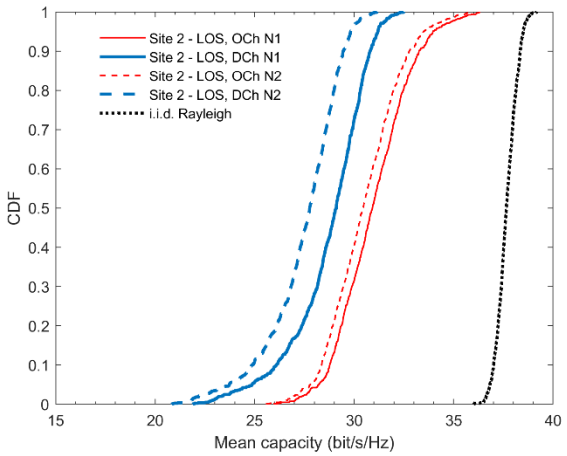

(c)

FIGURE 6. CDF of the capacity for 6 active UTs and 49 elements at the BS, considering a SNR of 10 dB. (a) Site 1–LOS (UT_{1-6}). (b) Site 1– NLOS (UT_{7-17}). (c) Site 2–LOS (UT_{1-6}).

From the results, when the structure of the radio channel is kept without correcting the power imbalance, i.e. N2 normalization, it can be observed that the behavior of the ICN is very similar in all the environments and, it is the OCh which presents the highest ICN values, i.e., it presents less dispersion of its singular values than the DCh.

It is also observed that both channels show lower ICN values than theoretical ones.

C. SUM CAPACITY

Figure 6 represents the CDF of the sum capacity of the uplink MU-MIMO channels for the three propagation situations considered. The capacity has been obtained according to the model presented in section III for a SNR=10 dB, and considering six UTs simultaneously active. The CDF for a i.i.d. Rayleigh channel is also included in Fig. 6. It is observed that in all cases there is a considerable loss of capacity when compared with the theoretical channels and, this fact has also been observed in other measurement campaigns, such as [10], [22]. When using N2 and in the three scenarios, it is verified that there is a loss of capacity of the DCh against the OCh, as was expected by observing the behavior of the ICN values obtained in the all three cases. This loss of capacity is greater in the NLOS-Site 1 and LOS-Site 2 scenarios, compared to the LOS-Site 1 scenario. In fact, the loss of median capacity is of 1, 2.8, and 2.7 bit/s/Hz in each of them, respectively.

In the case of considering in the system model an ideal power control, i.e. using N1, the capacity reflects the change of the channel structure, as shown by analyzing the ICN. For this normalization, the sum capacity obtained in the Site 1-LOS situation improves over the original channel (N2) for both DCh and OCh. However, the improvement is considerably smaller for the OCh, and the capacity of the DCh exceeds that obtained for the OCh. For the other two environments, the capacity obtained with N1 is always greater than the value achieved with N2 although, unlike the first case, the capacity of the OCh is greater than for the DCh.

V. CONCLUSION

In an indoor MU-MIMO channel, usually rich in scattering, the use of directional antennas at the BS array will result in a decrease in multipath components, at least in most situations. This fact in turn has two fundamental consequences on the channel: on the one hand, its frequency selectivity is reduced, and on the other, the orthogonality between the subchannels of different UTs is also reduced. A third effect of using directional antennas is that, with the increase in the directivity of the antennas, the power imbalance between UTs increases with great probability. This fact gives rise to a greater dispersion of the singular values of the channel matrix and, consequently, to a decrease in the sum capacity.

In this work, we have experimentally quantified to what extent the use of directional antennas at the BS array affects an indoor MU-MIMO channel through its impact on three fundamental parameters: the coherence bandwidth, the channel matrix condition number, and the sum capacity of the uplink.

The B_C increases considerably with the use of directional antennas, both in LOS and NLOS situations. Only in one of the environments there is a percentage of 16.6% of DCh channels with lower B_C than for OCh. For LOS situations, the increase in B_C values is greater than in NLOS ones, which

can be explained by the fact that the ''line-of-sight'' direction is close to the main lobe of the directional antenna for most of the UTs.

Concerning the change in the structure of the channel matrix associated with the use of directive antennas instead of omnidirectional ones, it should be noted that there are two effects difficult to separate a priori: changes in the level of orthogonality and relative powers between sub-channels. In order to separate these effects on the sum capacity, we propose the use of two normalizations. One of them is a scalar operation (N2), which preserves the structure of the original channel, including the power imbalance. The second one (N1) corrects the power imbalance between sub channels and modifies the original structure of the channel matrix, which can be interpreted as the use of an ideal power control in the up-link.

Considering N2, which preserves the structure of the original channel, it can be observed how the use of directional antennas leads to a greater dispersion of the singular values of the channel matrix. This fact is observed in the ICN values obtained. It can be said that this effect is very similar in the two measured environments, in both LOS and NLOS situations. As a result, a loss in the sum capacity is observed and losses reach values between 1 and 2.8 bit/s/Hz.

Using N1, a balance between the powers received at the BS from each UT is established. In this case, the sum capacity improves for all the measured situations. This improvement is greater in the case of using directive than omnidirectional antennas. The results obtained in the Site1-LOS situation show how this improvement causes the capacity of the DCh channel to even exceed that of the OCh channel. However, in the other two environments, the opposite is true: although the power imbalance is corrected, DCh still have a lower capacity than OCh. This fact shows that, in these cases, the loss of capacity due to the loss of orthogonality of the DCh channels versus the OCh weighs more than the influence of power imbalance.

In general, we can conclude that the use of directive antennas increases the B_C of the radio channel, and makes it decrease the sum capacity of the up-link. If an ideal power control is performed, the loss of capacity is mitigated in some environments but not in others.

It would be interesting to carry out new measurement campaigns in other environments, frequency bands and considering antennas with different directivities, which could complement the conclusions drawn in this work.

REFERENCES

[1] *IMT Vision—Framework and Overall Objectives of the Future Development of IMT for 2020 and Beyond*, document Rec. ITU-R M.2083-0, 2015.

[2] G. J. Foschini and M. J. Gans, ''On Limits of wireless communications in a fading environment when using multiple antennas,'' *Wireless Pers. Commun.*, vol. 6, no. 3, pp. 311–335, Mar. 1998, doi: 10.1023/A:1008889222784.

[3] E. Telatar, ''Capacity of multi-antenna Gaussian channels,'' *Eur. Trans. Telecomm.*, vol. 10, no. 6, pp. 585–595, Nov./Dec. 1999.

[4] G. Caire and S. Shamai, ''On the achievable throughput of a multiantenna Gaussian broadcast channel,'' *IEEE Trans. Inf. Theory*, vol. 49, no. 7, pp. 1691–1706, Jul. 2003, doi: 10.1109/tit.2003.813523.

[5] S. Vishwanath, N. Jindal, and A. Goldsmith, ''Duality, achievable rates, and sum-rate capacity of Gaussian MIMO broadcast channels,'' *IEEE Trans. Inf. Theory*, vol. 49, no. 10, pp. 2658–2668, Oct. 2003, doi: 10.1109/tit.2003.817421.

[6] D. Gesbert, M. Kountouris, R. W. Heath, C.-B. Chae, and T. Salzer, ''Shifting the MIMO paradigm,'' *IEEE Signal Process. Mag.*, vol. 24, no. 5, pp. 36–46, Sep. 2007, doi: 10.1109/msp.2007.904815.

[7] T. L. Marzetta, ''Noncooperative cellular wireless with unlimited numbers of base station antennas,'' *IEEE Trans. Wireless Commun.*, vol. 9, no. 11, pp. 3590–3600, Nov. 2010, doi: 10.1109/twc.2010.092810.091092.

[8] E. Björnson, E. G. Larsson, and T. L. Marzetta, ''Massive MIMO: Ten myths and one critical question,'' *IEEE Commun. Mag.*, vol. 54, no. 2, pp. 114–123, Feb. 2016.

[9] T. E. Bogale and L. B. Le, ''Massive MIMO and mmWave for 5G wireless HetNet: Potential benefits and challenges,'' *IEEE Veh. Technol. Mag.*, vol. 11, no. 1, pp. 64–75, Feb. 2016, doi: 10.1109/MVT.2015.2496240.

[10] X. Gao, O. Edfors, F. Rusek, and F. Tufvesson, ''Massive MIMO performance evaluation based on measured propagation data,'' *IEEE Trans. Wireless Commun.*, vol. 14, no. 7, pp. 3899–3911, Jul. 2015, doi: 10.1109/twc.2015.2414413.

[11] F. Rusek, D. Persson, B. Kiong Lau, E. G. Larsson, T. L. Marzetta, and F. Tufvesson, ''Scaling up MIMO: Opportunities and challenges with very large arrays,'' *IEEE Signal Process. Mag.*, vol. 30, no. 1, pp. 40–60, Jan. 2013, doi: 10.1109/msp.2011.2178495.

[12] E. G. Larsson, O. Edfors, F. Tufvesson, and T. L. Marzetta, ''Massive MIMO for next generation wireless systems,'' *IEEE Commun. Mag.*, vol. 52, no. 2, pp. 186–195, Feb. 2014, doi: 10.1109/mcom.2014.6736761.

[13] P. Singhparihar, R. Saraswat, and S. Maheshwari, ''Energy and spectral efficiency of very large multiuser MIMO systems,'' *Int. J. Comput. Appl.*, vol. 111, no. 5, pp. 4–7, Feb. 2015, doi: 10.5120/19532-1175.

[14] M. Di Renzo, H. Haas, A. Ghrayeb, S. Sugiura, and L. Hanzo, ''Spatial modulation for generalized MIMO: Challenges, opportunities, and implementation,'' *Proc. IEEE*, vol. 102, no. 1, pp. 56–103, Jan. 2014, doi: 10.1109/jproc.2013.2287851.

[15] A. Ourir, K. Rachedi, D. T. Phan-Huy, C. Leray, and J. Rosny, ''Compact reconfigurable antenna with radiation pattern diversity for spatial modulation,'' in *Proc. Eur. Conf. Antennas Propag.*, Paris, France, 2017, pp. 3038–3043.

[16] M. A. Jensen and J. W. Wallace, ''A review of antennas and propagation for MIMO wireless communication,'' *IEEE Trans. Antennas Propag.*, vol. 52, no. 11, pp. 2810–2824, Nov. 2004.

[17] J. D. Boerman and J. T. Bernhard, ''Performance study of pattern reconfigurable antennas in MIMO communication systems,'' *IEEE Trans. Antennas Propag.*, vol. 56, no. 1, pp. 231–236, Jan. 2008.

[18] J. Wallace and M. Jensen, ''Mutual coupling in MIMO wireless systems: A rigorous network theory analysis,'' *IEEE Trans. Wireless Commun.*, vol. 3, no. 4, pp. 1317–1325, Jul. 2004.

[19] P.-S. Kildal and K. Rosengren, ''Correlation and capacity of MIMO systems and mutual coupling, radiation efficiency, and diversity gain of their antennas: Simulations and measurements in a reverberation chamber,'' *IEEE Commun. Mag.*, vol. 42, no. 12, pp. 104–112, Dec. 2004.

[20] H. Hui, ''Influence of antenna characteristics on MIMO systems with compact monopole arrays,'' *IEEE Antennas Wireless Propag. Lett.*, vol. 8, pp. 133–136, 2009, doi: 10.1109/lawp.2009.2012446.

[21] J. R. Perez, R. P. Torres, L. Rubio, J. Basterrechea, M. Domingo, V. M. R. Penarrocha, and J. Reig, ''Empirical characterization of the indoor radio channel for array antenna systems in the 3 to 4 GHz frequency band,'' *IEEE Access*, vol. 7, pp. 94725–94736, 2019, doi: 10.1109/access.2019.2928421.

[22] R. P. Torres, J. R. Pérez, J. Basterrechea, M. Domingo, L. Valle, J. González, L. Rubio, V. M. Rodrigo, and J. Reig, ''Empirical characterisation of the indoor multi-user MIMO channel in the 3.5 GHz band,'' *IET Microw., Antennas Propag.*, vol. 13, no. 13, pp. 2386–2390, Oct. 2019, doi: 10.1049/iet-map.2018.6215.

[23] J. D. Parsons, ''Wideband channel characterization,'' in *The Mobile Radio Propagation Channel*, 2nd ed. London, U.K.: Wiley, 2000, ch. 6, pp. 164–189.

JESÚS R. PÉREZ received the B.Sc., M.Sc., and Ph.D. degrees in telecommunications engineering from the University of Cantabria, Spain, in 1996, 1999, and 2005, respectively. He joined the Department of Communications Engineering, University of Cantabria, in 1999, and was awarded a Graduate Research and a Postdoctoral Grant, in 2002 and 2006, respectively. He became an Associate Professor, in 2009. His research interests include computational electromagnetics, antenna measurement techniques, radio propagation, and optimization methods.

RAFAEL P. TORRES received the M.S. degree in physics from Granada University, Spain, in 1986, and the Ph.D. degree in telecommunications engineering from the Polytechnic University of Madrid (UPM), in 1990. He became an Associate Professor with the Department of Communications Engineering, University of Cantabria, Spain, where he is currently a Full Professor in signal processing and communications engineering. His fundamental lines of research have been the development of numerical methods for the analysis and design of antennas, application of high frequency techniques for simulation and analysis of the radar section, as well as the design of radar systems. From the end of the nineties, his research focuses on the study, modeling, and measurement of the radio channel and the analysis of its impact on mobile and wireless communications systems. His main achievements focus on the development of ray-tracing methods to simulate the radio channel in complex propagation environments, on the experimental characterization of the channel, both SISO and MIMO, and on the development of space-time coding techniques.